ORIGINAL ARTICLE

Impact of solar radiation pressure models on earth rotation parameters derived from BDS

Yaquan Peng[1] · Yidong Lou[1] · Xiaolei Dai[1] · Jing Guo[1] · Chuang Shi[2]

Abstract

Earth rotation parameters (ERPs) are susceptible to absorbing the spurious effects from global navigation satellite system constellation characteristics and orbit modeling deficiencies, especially the deficiencies in the solar radiation pressure (SRP) models. This study investigates the impact of SRP modeling on the ERP estimation derived from BeiDou Navigation Satellite System (BDS). The adjusted optical properties are adopted in an a priori box-wing model and jointly used with the extended CODE orbit model (ECOM) for BDS ERP estimation. The BDS-derived ERPs are assessed by comparing them with International Earth Rotation and Reference Systems Service (IERS) 14C04 product. Our processing results of 3 years (2019–2021) show that the mean offsets of BDS-derived ERPs are nearly not affected by the a priori SRP model. However, the standard deviation (STD) is improved by approximately 20% for pole coordinates and their rates when considering an a priori box-wing model together with the ECOM1 (5 parameters). The a priori bow-wing model mitigates most spurious signals in the pole coordinate spectrum. It is noticeable that the BDS-derived ERPs are also affected by the system-specific spurious signals. The visible signals at the 3rd harmonics of draconitic year in the pole coordinates are related to the 3-plane constellations. The signal at the 2nd harmonics of the draconitic year for BDS-derived excess length of day (ΔLOD) estimates is significantly larger than that of the GPS-derived. Additionally, the extension of the orbital arc in the BDS processing from 1 to 3 day is beneficial for the ERP quality. When switching to a 3-day arc length, the improvement of the ERP quality is about 28, 15 and 50 for X-pole, Y-pole coordinates and Δ LOD, respectively. The STD is more than 3 times better than that of 1-day arc solutions for pole coordinate rates. The STD of the 3-day arc length BDS-derived ERPs with respect to the IERS 14C04 product reaches about 40 μas, 100 μas/day, 9 μs for pole coordinates, pole coordinate rates and Δ LOD, respectively.

Keywords BDS · Earth rotation parameters · Solar radiation pressure · Spurious signals

Introduction

External forces (the gravitational forces of the sun, moon and planets) and internal dynamical processes (the exchange of angular momentum between the earth's core, hydrosphere, and atmosphere) exert torques on the solid Earth, resulting in changes in the earth's rotation (Gross et al. 2003). Conventionally, the irregularities of the earth's rotation are described by the Earth Orientation Parameters (EOPs, www.ggos.org), which are composed of the celestial pole offsets, earth rotation angle (linearly proportional to universal time (UT1), the actual observable is UT1-coordinated universal time (UTC)), and polar motion. Technically, the EOPs are transformation parameters connecting the International Celestial Reference Frame (ICRF) and the International Terrestrial Reference Frame (ITRF). The celestial pole offsets describe the variation of the earth's axis in space by external gravitational forces (generally called nutation and precession), which can be accurately obtained using the IAU2000/2006 model (Petit and Luzum 2010). However, the causes of the polar motion and earth rotation angle are more complicated and can be estimated through measurement data in most cases (Gross et al. 2003). The polar motion and earth rotation angle are usually called the Earth Rotation Parameters (ERPs), which include X-, Y-pole coordinates and their rates, UT1-UTC and its rate named excess length of day ($\Delta\text{LOD} = \backslash - \frac{\text{d(UT1−UTC)}}{\text{d}t} * 86400\text{s}$). A global

✉ Xiaolei Dai
  xldai@whu.edu.cn

1 GNSS Research Center, Wuhan University, Luoyu Road 129, Wuhan 430079, Hubei, China

2 School of Electronic and Information Engineering, Beihang University, Xueyuan Road 37, Beijing 100191, China

navigation satellite system (GNSS) is the primary technique for deriving ERPs except for UT1-UTC due to the globally distributed ground receivers and a large number of satellites. The GNSS technique cannot determine the absolute UT1 as the singularities between UT1 and the orbital elements, especially the right ascension of the ascending node (Thaller et al. 2007). However, the changes of UT1-UTC (Δ LOD) can be determined from GNSS measurements (Bizouard et al. 2019).

ERPs are estimated together with GNSS satellite orbits, which are susceptible to absorbing the spurious effects introduced by GNSS constellation characteristics and orbit modeling deficiencies. On the one hand, Zajdel (2020) demonstrated that the quality of ERPs derived from GPS-only is superior to that of GLONASS-only and Galileo-only, which may be related to the number of orbital planes (6 for GPS, 3 for GLONASS and Galileo). Fewer orbital planes may attribute to deteriorations in the estimation of pole coordinates (Scaramuzza et al. 2018). The ERPs derived from different systems absorbed system-related errors and spurious signals, such as the strong signal at the 3rd harmonic of the draconitic year (the repeat period of the GNSS constellation w.r.t. the Sun) in the pole coordinate series from the 3 planes system. The combination of multi-GNSS mitigates these errors and improves the estimated ERP quality (Zajdel et al. 2020). On the other hand, the degradation of ERP quality mainly originated from orbit modeling deficiencies. As the correlation of ERP and orbital parameters, the errors in the orbit model will introduce spurious orbit-related signals into the estimated ERPs, especially the deficiencies of the solar radiation pressure (SRP) model. Rodriguez-Solano et al. (2014) indicated that the GPS draconitic signals in the pole coordinate rates are significantly reduced when using the adjustable box-wing model (ABW, Rodriguez-Solano et al. 2012a) for SRP modeling instead of a purely empirical extended CODE orbit model (ECOM). Similarly, Lutz et al. (2016) indicated that the ERPs derived from 3 day arc solutions are typically better than those derived from the 1-day arc solutions. The improvement in pole coordinates quality benefits from the higher accuracy of parameter estimates, such as the SRP parameters. Zajdel et al. (2020) suggested that the hybrid SRP model of combining both empirical and physical models is beneficial for the ERP quality. Unfortunately, the above studies did not cover the analyses of the BeiDou Navigation Satellite System (BDS), which comprises 3 orbital planes and uses the combined constellation of Medium Altitudes Earth Orbit (MEO), Inclined Geosynchronous Orbit (IGSO), and Geostationary Earth Orbit (GEO) satellites. The BeiDou Regional Navigation Satellite System (BDS-2) and the BeiDou Global Navigation Satellite System (BDS-3) satellites are working together to support global positioning, navigation, and timing (PNT) services (Yang et al. 2020). In the initial stages, the pole coordinates derived from BDS-2 only reached the level of mas due to the poor distribution of the tracking network and the small number of satellites (Xu et al. 2014). Currently, the BDS constellation has reached the number of 45 satellites in space and more than 200 International GNSS Service (IGS; Johnston et al. 2017) network stations that can track BDS-2 and BDS-3 satellites by the middle of 2021. Although good geometry and adequate observations are realized, the imperfect SRP model restricts the quality of ERPs derived from BDS. Due to the lack of accurate satellite metadata, the purely empirical reduced extended CODE orbit model (ECOM1) is widely used in BDS precise orbit determination (POD) and geodetic parameters estimation. However, the ECOM1 was firstly developed for GPS satellites with cube bodies (Springer et al. 1999), which may not be suitable for BDS satellites, especially for the BDS-3 satellites with cuboid bodies. The SLR residuals of BDS-2 and BDS-3 satellite orbits show systematic error dependency on the sun elongation angle when the ECOM1 is applied (Wang et al. 2022; Duan et al. 2022). Although adding higher-order periodic parameters in empirical models can better absorb the SRP perturbation such as ECOM2 (Arnold et al. 2015), the higher-order periodic terms degrade the quality of geodetic parameters estimation (Bury et al. 2019). Therefore, the analytical box-wing model is widely applied. But the analytical box-wing model alone is not sufficient without additional correction model parameters (Bury et al. 2020). Using the priori box-wing model and estimating empirical parameters reduces orbital errors and spurious signals in the spectra analysis of the pole coordinate estimates (Zajdel et al. 2020). However, Wang et al. (2022) found that the box-wing model as an a priori model cannot eliminate the systematic errors of SLR residuals for BDS-2 IGSO and MEO satellites. They pointed out that the systematic errors of SLR residuals for BDS-2 IGSO/MEO satellites vanished when considering the thermal re-radiation force. Better orbit accuracy can be realized for BDS-3 satellites by employing an a priori box-wing model (Duan et al. 2022). Duan et al. (2022) presented the performance of BDS satellites for the ERPs estimation by using different SRP models. The improvement of ERP quality was not significant after introducing an a priori model compared with the great improvement of orbit quality. Although the Bernese software is adopted, the accuracy of BDS-derived ERPs is significantly worse than that derived from other navigation systems, especially the performance of Δ LOD, according to Duan et al. (2022) and Zajdel et al. (2020). Moreover, the spectra analysis of the ERPs derived from BDS was not mentioned. The impact of SRP models on ERPs in BDS processing has not been fully investigated. Finally, the observation period of most BDS satellites is close to 3 years and their contributions to ERP estimation should be studied.

Motivated by Zajdel et al. (2020), we investigate the quality of the BDS-derived ERP estimation by using different SRP models in this study. We first analyze the formal errors of the ERP estimates and the correlations between the orbit parameters and ERPs. Next, the performance of BDS-derived ERP estimation is assessed by comparing it with the reference values of the IERS 14C04 product. Finally, the spectra analysis is also studied for the specific signals in BDS-derived ERPs.

Methodology

This study performed the computations on Position And Navigation Data Analyst (PANDA) software. Observations from DOY 150, 2019 to DOY 300, 2021 were collected from the Multi-GNSS Experiment (MGEX; Montenbruck et al. 2017) networks of about 125 global stations (distributed in Fig. 1). The ERPs are estimated simultaneously with the orbit parameters and station coordinates. The "one-step" method is adopted in the BDS POD and the processing details and the overview of the background models are summarized in Table 1. The ERPs are parametrized as piecewise linear with a temporal resolution of 24 h. The ERPs and their rates are calculated for each day at 12 h UTC, which is consistent with the IGS product. In addition, the UT1-UTC has tightly constrained to IERS 14C04 values at the first epoch due to the singularity between orbital parameters and UT1-UTC. The ERPs are estimated based on 1 and 3 day orbital arc solutions, respectively. For any two adjacent 3 day solutions, the orbit solutions are shifted by 1 day. A strong constraint is introduced at common nodes at midnights in the 3 day solution, making the ERPs continuous at the boundaries of the day (Lutz et al.2016). Only the ERP of the middle day in a 3 day solution is extracted and evaluated.

Table 2 describes five solutions for assessing the impact of SRP models on the ERP estimates derived from BDS. Moreover, the ERPs derived from GPS-only were also computed for comparison. In the GPS solution, we choose the different variations of the ECOM model for different satellite
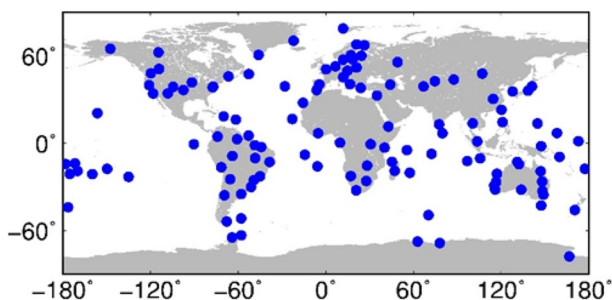

Fig. 1 Distribution of the 125 MGEX stations

blocks according to the recommendation of the IGS repro3 (http://acc.igs.org/repro3/repro3.html). We employed purely empirical ECOM and hybrid models in the BDS solutions. The hybrid model combines a physically interpreted box-wing and empirical ECOM model, which benefits the orbit and ERP quality (Duan et al. 2022). For better consistency with our software, we adjusted the initial properties of the box-wing model provided by Zhao et al. (2022). The box-wing model is developed on the satellite-fixed coordinate system ($+Z$-axis points to the center of the Earth, Y-axis is along the rotation axis of solar panels and $+X$-axis completes the right-handed frame with the positive direction pointing to the hemisphere illuminated by the Sun; Rodriguez-Solano et al. 2012a). In this study, nine parameters, including solar panels (SP) scaling factor, the absorption plus diffuse reflection (AD) and the specular reflection (R) parameters of illuminated $+Z$, $-Z$ and $+X$ panels ($+ZAD, +ZR, -ZAD, -ZR, +XAD, +XR$), solar panel rotation lag, and Y-bias acceleration, were estimated for all BDS satellites. Moreover, the extra thermal re-radiation scale factor K for the $+X$ panel was estimated for BDS-2 IGSO and MEO satellites to absorb the incorrect thermal radiation pressure (Wang et al. 2022). Noteworthy, BDS GEO satellites were not involved due to their poor orbit accuracy. BDS-3 IGSO satellites (space vehicle number (SVN) C220, C221, C222) are equipped with hexagonal and circle antennas with unknown metadata on the X surfaces and were also not considered (Zhao et al. 2022). The estimated optical properties and the mean formal errors are shown in Table 3, 4 and 5. The physical constraint AD + R = 1 has not been imposed in the estimation of satellite body panels and thus we can evaluate whether the summed estimates are equal to 1. The deviations of the summed optical properties from 1 on $+X$ panel are larger than that of other panels in Fig. 2, especially for BDS-2, CAST2 (satellites developed by China Academy of Space Technology) and SECM2 (satellites developed by Shanghai Engineering Center) satellites. This might be caused by the inaccurate dimension information of the satellite $+X$ panel. However, the adjusted optical properties are then adopted in the a priori box-wing model, jointly used with the ECOM in the BDS POD process. The linear dependence of SLR residuals on the elongation angle is vanished, which is in accord with the results of other research (Wang et al. 2022; Duan et al. 2022).

Results

In this part, we discuss the quality of ERP estimates. Firstly, we analyzed the formal errors and correlations between the estimated parameters. Then the X- and Y-pole coordinates, their rates, and Δ LOD from different solutions are compared with the IERS 14C04 product. To

Table 1 Description of the processing strategy

Items	Adopted processing strategy
Basic observables	Ionosphere-free (IF) combinations of code and phase observations. BDS B1I + B3I; GPS: C1C/L1C and C1W/L2W for L1 band; C2L/L2L and C2W/L2W for L2 band
Code biases	BDS-2: Wanninger and Beer (2015); GPS: corrected by the products provided by CODE
Time span	DOY 150, 2019 to DOY 300, 2021
Estimator	LSQ in batch mode
Processing interval	300 s
Arc length	1-/3-day
Attitude mode	GPS: yaw-steering + eclipse attitude model (Kouba 2008; Dilssner et al. 2011); BDS C007-C010 satellites: yaw-steering + orbit-normal attitude mode ($|\beta| < 4°$); Other BDS satellites: yaw-steering + eclipse attitude model (Dilssner et al. 2018)
Satellite antenna phase center offsets (PCO) and variations (PCV)	BDS PCO: http://www.beidou.gov.cn BDS PCV: ignored GPS: igs14.atx
Receiver antenna PCO and PCV	BDS: igs14.atx; If the values of B1/B3 do not exist, the values of GPS L1/L2 are used for correction GPS: igs14.atx
Antenna thrust	GPS: Rodriguez-Solano et al. (2012a, b); BDS-2: Steigenberger et al. (2018); BDS-3: Steigenberger and Thoelert (2020)
Earth albedo radiation	GPS: Rodriguez-Solano et al. (2012b); BDS: Zhao et al. (2022)
A priori reference frame	IGS14 (Rebischung and Schmid 2016)
Station coordinate	Tight constraints to the igs{week}.snx ($\sigma \leq 10^{-3}$m)
Solid earth tides, pole tides, and ocean tides	IERS 2010 (Petit and Luzum 2010); FES2004 (Lyard et al. 2006) for ocean tides
Tropospheric delay	Saastamoinen model and meteorological data from Global Pressure and Temperature (Saastamoinen 1972; Boehm et al. 2007) + Global Mapping Function (Boehm et al. 2006); Zenith wet delay and gradient parameters are parametrized as piecewise constants with a temporal resolution of 2 and 24 h, respectively
Earth rotation parameters	Precession and Nutation: IAU2006A (Free Core Nutation is not modeled); A priori ERPs: IERS 14C04. A priori-constraints: polar motion (100 mas); polar motion rates (10 mas/day); UT1-UTC (100 μs); Δ LOD (2 ms); Diurnal and sub-diurnal variations: corrected by IERS 2010 (Ray et al. 1994)
Pseudo-stochastic pulses	Every noon and midnight epochs in the along-track (10^{-8}m/s), cross-track (10^{-9}m/s) and radial (10^{-9}m/s) directions in 3 day solutions

Table 2 Description of the solutions

Solution	Satellites	Description of SRP models
ECOM1	BDS-2, BDS-3	ECOM1 (5 parameters)
BW + ECOM1	BDS-2, BDS-3	ECOM1 (5 parameters) with an a priori box-wing model
BWmix + ECOM1	BDS-2	ECOM1 + X thermal re-radiation force
	BDS-3	ECOM1 (5 parameters) with an a priori box-wing model
ECOM2	BDS-2, BDS-3	ECOM2 (7 parameters)
BW + ECOM2	BDS-2, BDS-3	ECOM2 (7 parameters) with an a priori box-wing model
GPS	BLOCK IIA/IIR/III	ECOM2 (7 parameters)
	BLOCK IIF	ECOM1 (5 parameters)

reduce the interpolation errors, the IERS 14C04 series sampling at the noon epoch is adopted to compare pole coordinates and ΔLOD (ftp://hpiers.obspm.fr/iers/eop/eopc04/eopc04.dX_dY.12h.84-now). As no pole coordinate rates are available in the IERS 14C04 product, the reference values are calculated by the difference of pole coordinates of two adjacent midnight epochs (ftp://hpiers.obspm.fr/iers/eop/eopc04/eopc04.62-now).

Table 3 Adjusted properties and mean formal errors of BDS-2 and CAST1 groups. The BDS-2 includes BDS-2 IGSO/MEO satellites and the CAST1 group includes BDS-3 C201, C202, C205, C206, C209, C210, C213, C214, C218, C219, C227, C228 satellites

Panel	BDS-2		CAST1	
	AD	R	AD	R
$+X$	0.194 ± 0.054	0.329 ± 0.038	0.320 ± 0.051	0.569 ± 0.040
$+Z$	0.498 ± 0.036	0.259 ± 0.041	0.214 ± 0.035	0.731 ± 0.045
$-Z$	0.492 ± 0.035	0.501 ± 0.042	0.557 ± 0.036	0.410 ± 0.044
SP	0.720 ± 0.000	0.378 ± 0.014	0.920 ± 0.000	0.233 ± 0.010

Formal errors of ERP estimates

Figure 3 draws the time series of the parameter errors from the respective solutions. The parameter errors derived from BDS solutions are slightly larger before the beginning of 2020 because of the fewer BDS satellites and stations (Fig. 4). Table 6 summarizes the median of formal errors for each solution. As more observations are used, the formal errors of pole coordinates in 3 day solutions are about 1.7 times smaller than those in 1 day solutions. The median is smaller by about 30% for the GPS solution than that for BDS solutions. In addition, a strong correlation with β can be identified for Δ LOD errors from all BDS 1-day solutions, while it is insignificant for X-pole coordinate errors, as shown in Fig. 3. The largest errors occur at the β zero-crossing points and are still visible, although the hybrid SRP modeling is applied. However, these characteristic patterns are significantly reduced in 3 day arc solutions. The degradation of Δ LOD at the β zero-crossing points in 1 day arc solutions may be caused by the correlation between the estimated parameters. Figure 5 shows the correlations between the Δ LOD and the orbit parameters for 1-day and 3 day solutions. At the epoch of the equal β point, i.e., when two orbital planes have the same β angle, the correlation between Δ LOD and orbital parameters is not visible in the 1 day solution. However, the significant correlation is up to 0.6 at the β zero-crossing point. The

Table 5 Thermal re-radiation estimates and mean formal errors of BDS-2 IGSO and MEO satellites

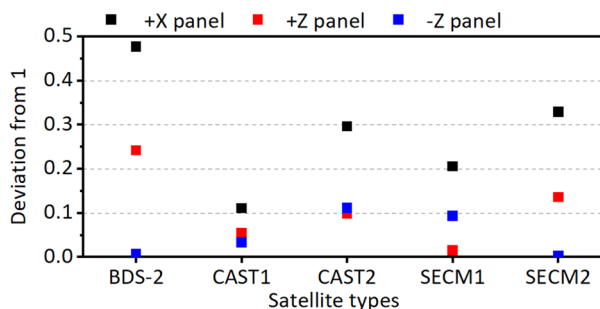| SVN	C005	C007	C008	C009	C010
$K(nm/s^2)$	1.10 ± 0.4	4.49 ± 0.3	3.83 ± 0.3	1.45 ± 0.4	3.35 ± 0.2
SVN	C012	C013	C015	C017	C019
$K(nm/s^2)$	4.21 ± 0.3	4.20 ± 0.4	2.63 ± 0.2	3.16 ± 0.3	1.77 ± 0.3

Fig. 2 The deviation from 1 of the summed optical properties for satellite panels

extension of the orbital arc decreases most of these correlations and the correlations are not larger than 0.3.

Pole coordinate

Figure 6 shows the time series of pole coordinate differences with respect to the IERS 14C04 product. The differences of GPS-derived pole coordinates vary in the range of a few dozens of μas and are stable over the whole time. However, the differences of BDS-derived pole coordinates are about two times larger than those of the GPS solution. The accuracy of pole coordinates derived from BDS also changes with the development of BDS constellations, which is slightly poorer before the beginning of 2020 because of the fewer observations. Table 7 summarizes the mean offsets and STD values of the differences. For the BDS-derived pole coordinates, the mean offsets using different SRP models are almost at the same level, which are about -35 and -15 μas for X- and

Table 4 Adjusted properties and mean formal errors of CAST2, SECM1 and SECM2 groups. The CAST2 group includes BDS-3 C222, C223 satellites, the SECM1 group includes BDS-3 C203, C204, C207, C208, C211, C212 satellites, and the SECM2 group includes C215, C216, C225, C226 satellites

Panel	CAST2		SECM1		SECM2	
	AD	R	AD	R	AD	R
$+X$	0.230 ± 0.055	0.473 ± 0.047	0.136 ± 0.056	0.658 ± 0.050	0.075 ± 0.047	0.595 ± 0.043
$+Z$	0.086 ± 0.042	0.988 ± 0.050	0.549 ± 0.032	0.436 ± 0.042	0.610 ± 0.029	0.526 ± 0.037
$-Z$	0.919 ± 0.042	0.193 ± 0.051	0.186 ± 0.032	0.720 ± 0.042	0.204 ± 0.030	0.800 ± 0.036
SP	0.920 ± 0.000	0.325 ± 0.012	0.920 ± 0.000	0.275 ± 0.017	0.920 ± 0.000	0.397 ± 0.018

Fig. 3 Formal errors of the *X*-pole coordinate and LOD estimates from different solutions for 1 day arc (blue lines) and 3 day arc (red lines). Gray dashed lines denote the sun elevation angles above orbital planes. Vertical cyan lines point to the epochs of the β zero-crossing point and the equal β point (two orbital planes have the same β angel) of BDS constellation, which are further elaborated in Fig. 5
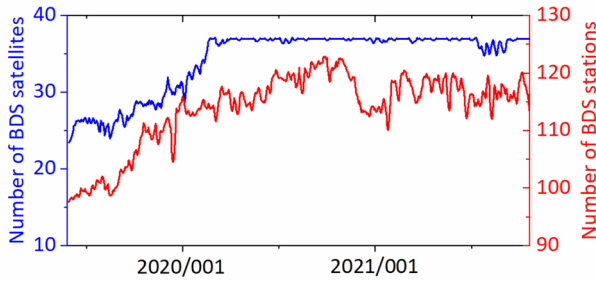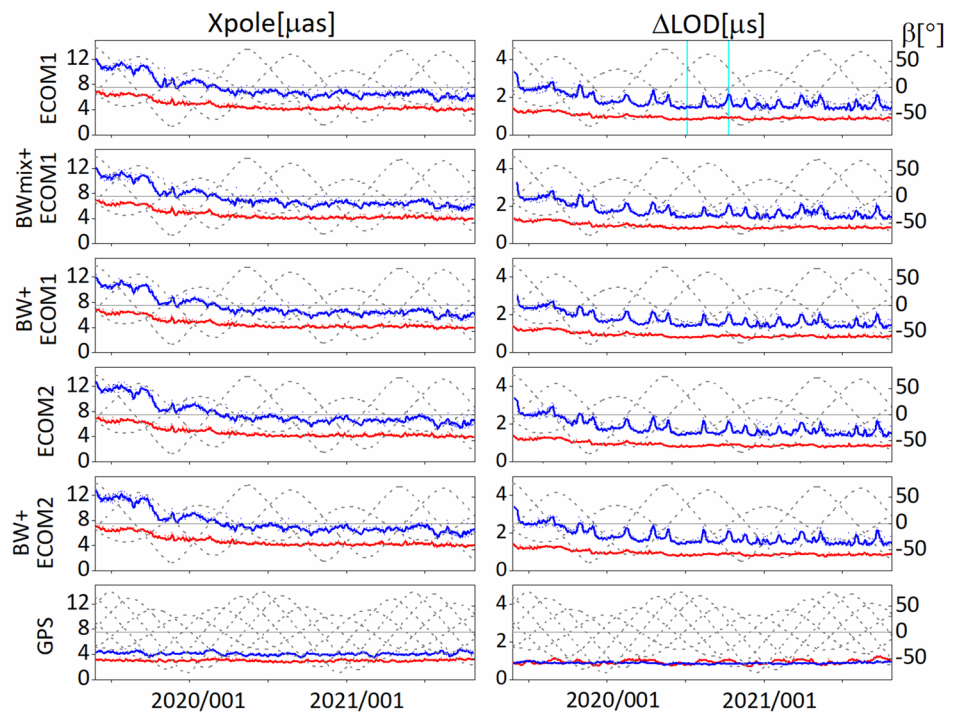

Fig. 4 Number of BDS satellites and stations in the POD processing

Y-pole coordinates based on 1 day arc solutions, respectively. The mean offsets of 3 day arc solutions do not change significantly for the *X*-pole coordinate. Nevertheless, the mean offsets of the *Y*-pole coordinate change from − 15 to 17 μs when a 3 day arc solution is applied. A similar pattern also

can be found in the GPS-derived pole coordinate solutions. Two possible reasons account for the obvious mean offsets in the BDS-derived pole coordinates. The first reason is the system-specific offset due to the different numbers and design of orbital planes for the GPS and BDS constellations (Zajdel et al. 2020). The mean offsets of the GPS-derived pole coordinates are close to zero in Table 7 since the GPS results dominate the pole coordinates in IERS 14C04 product. The other might be caused by the lack of accurate PCO/PCV corrections for BDS satellites in the processing. Moreover, the BDS-derived pole coordinates will be dominated by the contribution of BDS-3 due to its 24 MEO satellites. In the case of 1 day arc BDS-derived solutions, as in line with the orbit quality, the ECOM1 solution results are scattered with an STD of 77 and 58 μas for *X*- and *Y*-pole coordinates, respectively. The BW + ECOM1 solution leads to a decrease of approximately 30% for X-pole coordinate and 17% for Y-pole coordinate in the STD compared to the ECOM1

Table 6 Median of the formal errors for the respective solutions

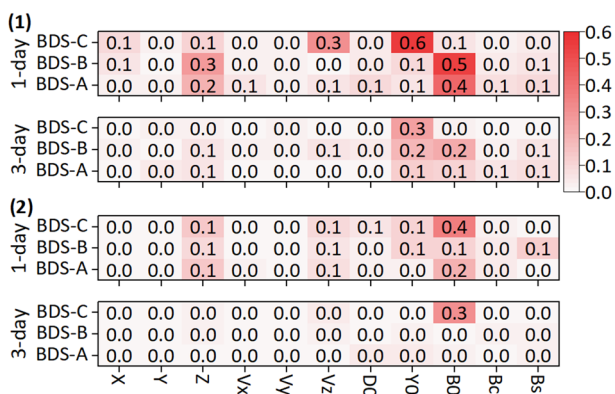|	X pole coordinate (μas)		Y pole coordinate (μas)		Δ LOD (μs)	
	1 day	3 day	1 day	3 day	1 day	3 day
ECOM1	6.9	4.3	6.4	4.2	1.7	0.9
ECOM2	7.1	4.3	6.6	4.2	1.7	0.9
BW + ECOM1	6.7	4.3	6.3	4.1	1.6	0.9
BW + ECOM2	7.0	4.3	6.5	4.2	1.7	0.9
BWmix + ECOM1	6.8	4.3	6.4	4.2	1.6	0.9
GPS	4.1	3.0	3.5	2.9	0.9	0.9

Fig. 5 Correlations between Δ LOD and orbit parameters for 1 and 3 day solutions for the ECOM1 solution (Fig. 3). (1) The correlations at the epochs of the β zero-crossing point (2) The correlations at the epochs of the equal β point (Fig. 3). One satellite per BDS orbital plane is selected. BDS-A, BDS-B and BDS-C represent different orbital planes, respectively
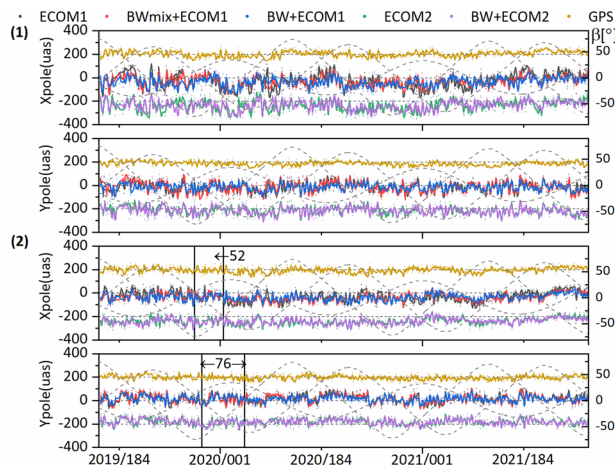

Fig. 6 Time series of pole coordinate differences with respect to IERS 14C04 product. (1) The 1 day arc solutions (2) The 3 day arc solutions. These series are smoothed using the moving average filter with a 5 day window. The colored lines represent the smoothed lines. The ECOM2, BW + ECOM2, and GPS solutions are shifted by −200, −200, and 200 μas for a better display. Gray dashed lines denote the sun elevation angles above orbital planes. The labels 52 and 76 are the repeating period of the β zero-crossing point and the equal β point for BDS, respectively

solution. The STD is 54, 59, 55, 61 μas for the *X*-pole coordinate and 48, 51, 48, 50 μas for the *Y*-pole coordinate, for the solutions of BW + ECOM1, ECOM2, BW + ECOM2 and BWmix + ECOM1, respectively. Although the BWmix + ECOM1 solution brings smaller SLR residuals for BDS-2 satellite orbits, the STD of residuals is worse than the BW + ECOM1 solution both in *X*- and *Y*-pole coordinates. The results of the BW + ECOM2 solution are comparable with the ECOM2 solution. Furthermore, the differences for

Table 7 Mean offsets and STD values of the pole coordinate differences with respect to IERS 14C04

	1 day arc		3 day arc	
	Mean	STD	Mean	STD
X pole coordinate (μas)				
ECOM1	− 28	77	− 30	52
ECOM2	− 40	59	− 39	41
BW + ECOM1	− 36	54	− 33	41
BW + ECOM2	− 39	55	− 39	41
BWmix + ECOM1	− 33	61	− 34	44
GPS	1	33	− 5	32
Y pole coordinate (μas)				
ECOM1	− 15	58	16	52
ECOM2	− 16	51	19	42
BW + ECOM1	− 15	48	16	42
BW + ECOM2	− 16	50	19	42
BWmix + ECOM1	− 15	59	15	50
GPS	− 13	24	− 1	27

the corresponding solutions become smaller when a 3 day arc is adopted in Fig. 6. The improvement of STD is about 28 and 15% for *X*- and *Y*-pole coordinates compared to 1 day arc solutions, respectively. This decrease of STD in 3 day arc solutions is attributed to more observations and the reduction of correlations between parameters (Lutz et al. 2016). Finally, the best STD for *X*- and *Y*-pole coordinates derived from BDS reaches 41 and 42 μas, respectively. However, the STD of GPS solution is 32 and 27 μas for the *X*- and *Y*-pole coordinates, respectively. During the same period, the STD of differences between CODE final ERP products (ftp://ftp.aiub.unibe.ch/CODE/{year}/COD{week}7.ERP.Z) and IERS 14C04 product is 33 and 26 μas for the *X*- and *Y*-pole coordinates, respectively. Likewise, the STD for IGS final ERP products (ftps://gdc.cddis.eosdis.nasa.gov/gps/products/{week}/igs{week}7.erp.Z) reaches 23 and 15 μas for the *X*- and *Y*-pole coordinates, respectively. The better statistical values obtained for GPS-derived pole coordinates may be attributed to more orbital planes, a stable number of satellites, and fewer orbit modeling issues.

In addition, assuming that the IERS 14C04 series are true values, the real signals in the ERP estimates will be eliminated by subtracting. The remaining amplitudes greater than the noise level in the spectrum analysis can be interpreted as introduced by the specific processing, such as draconitic year errors. Figure 7 shows the spectral analysis of the time series of the differences between the estimated pole coordinates and the IERS 14C04 product (the trends of the residuals between the ERP estimates and the IERS 14C04 series are moved). It can be seen that the spurious signals at the harmonics of the draconitic year are distinct in almost all solutions. The *X*-pole coordinate is more vulnerable to
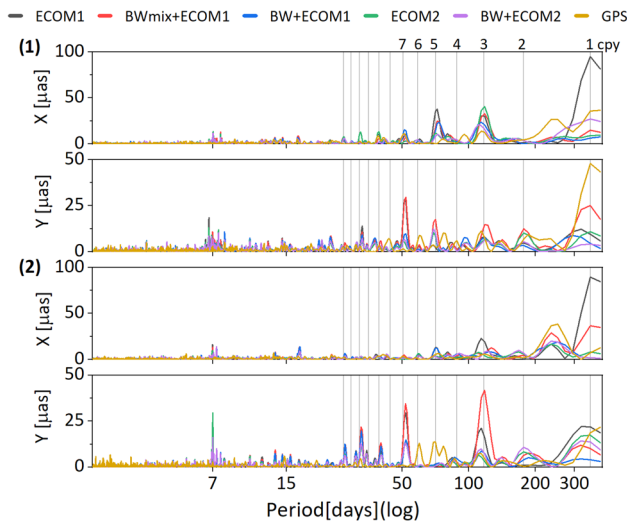
Fig. 7 Amplitude spectra of the differences between the estimated *X*- and *Y*-pole coordinates and the IERS 14C04 series. (1) The 1 day arc solutions (2) The 3 day arc solutions. The vertical gray lines represent the first 14 harmonics of a draconitic year (~353 days) Polar coordinate rate

Table 8 Mean offsets and STD values of the pole coordinate rate differences with respect to IERS 14C04

	1 day arc		3 day arc	
	Mean	STD	Mean	STD
X pole coordinate rates (µas/day)				
ECOM1	104	347	7	102
ECOM2	96	316	7	96
BW + ECOM1	104	272	6	96
BW + ECOM2	86	314	6	97
BWmix + ECOM1	102	328	8	98
GPS	91	132	− 5	80
Y pole coordinate rates (µas/day)				
ECOM1	− 52	398	2	108
ECOM2	− 36	360	0	104
BW + ECOM1	− 40	326	3	103
BW + ECOM2	− 24	354	0	104
BWmix + ECOM1	− 53	342	5	104
GPS	− 6	164	1	85

spurious signals than the *Y*-pole coordinate, especially the signal at the 3rd harmonics of the draconitic year with an amplitude of about 35 µas. Some similar spurious signals appear in all BDS-only solutions, which may be related to system-specific errors. The apparent signals at the 3rd harmonics of the draconitic year in the pole coordinates may be associated with the 3-plane constellations for BDS, which are almost invisible in pole coordinates derived from GPS. What is noteworthy is that the spectra also show the clear peaks at the 5th (about 70 days) and 7th (about 52 days) harmonics of the draconitic year. Figure 6 shows that the *β* zero-crossing points of consecutive orbital planes and the same *β* points between two orbital planes are repeated for 76 and 52 days, respectively. These two repeated periods may lead to the visible signals at the 5th and 7th harmonics of the draconitic year in ERP estimation (Zajdel et al. 2021). These signals are mitigated when the a priori box-wing model is applied. Although the 3 day arc solutions can mitigate most of these spurious signals, some of them are even increased by the errors accumulated over a long period. Moreover, visible spurious signals with a period close to 7.4 days and an amplitude of about 10 µas in *X*- and *Y*-pole coordinates may be introduced by the resonance between earth rotation and satellites revolution (12 h 50 min for BDS MEO satellites) according to Zajdel (2020). Several pronounced peaks around 7 days in all BDS-only solutions may relate to the orbit repeat period. According to the statistical results from Zou et al. (2021), the orbit repeat period of BDS-3 MEO satellites is about 7 days, which varies slightly among individual satellites. As the different SRP model solutions for

BDS, the a priori bow-wing model mitigates the draconitic signals in the purely empirical SRP model solutions, especially for the signals at the 1st and 3rd harmonics of the draconitic year.

Pole coordinate rate are essential for the prediction of pole coordinates. Table 8 summarizes the mean offsets and STD values of residuals for the *X*- and *Y*-pole coordinate rates. In the case of 1 day arc BDS-derived solutions, the quality of the estimated pole coordinate rates is quite uncertain (as reported in Lutz et al. 2016). The mean offset reaches approximately 100,− 40 µas/day for *X*- and *Y*-pole rates and the STD exceeds 300 µas/day. The STD of BW + ECOM1 solution is reduced by 21% and 18% for *X*- and *Y*-pole coordinate rates compared to those of ECOM1 solution, respectively. The improvement of the estimated pole coordinate rates is significant when switching to the 3 day arc. The mean offsets decreased to a few µas/day for all solutions. The STD is more than 3 times better than that of 1 day arc solutions and at the level of 102, 96, 96, 97, 98 µas/day for *X*-pole coordinate rate, 108, 104, 103, 104, 104 µas/day for *Y*-pole coordinate rate, for ECOM1, ECOM2, BW + ECOM1, BW + ECOM2, BWmix + ECOM1 solutions, respectively. Even for GPS solution, a factor of about 2 improvements is brought in 3 day arc solutions. The spectral analysis of the residuals of the estimated pole coordinate rates is illustrated in Fig. 8. Similar draconitic signals in the series of pole coordinates are also visible in Fig. 7. In a circular polar motion of angular velocity ω, we may expect that $\dot{y} = +\omega x$ and $\dot{x} = -\omega x$ (ω is angular velocity of the earth rotation). Thus, the *Y*-pole coordinate rate has more spurious signals than the *X*-pole coordinate rate. The signal at the 3rd harmonics of the draconitic year is
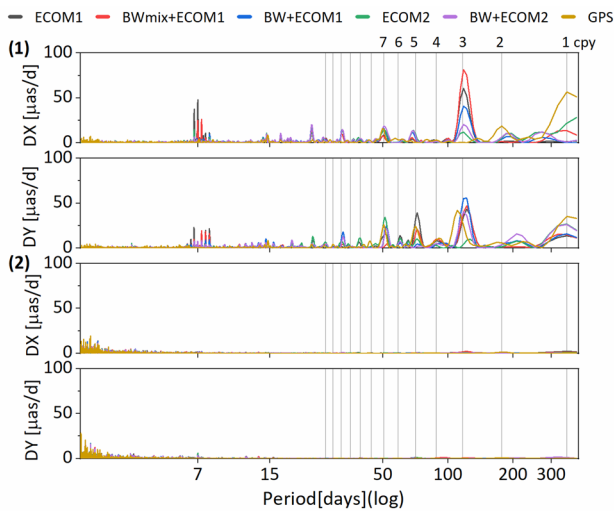
Fig. 8 Amplitude spectra of the differences between the estimated *X*-and *Y*-pole coordinate rates and the IERS 14C04 series. (1) The 1 day arc solutions (2) The 3 day arc solutions. The vertical gray lines represent the first 14 harmonics of a draconitic year (~353 days) Excess length of day
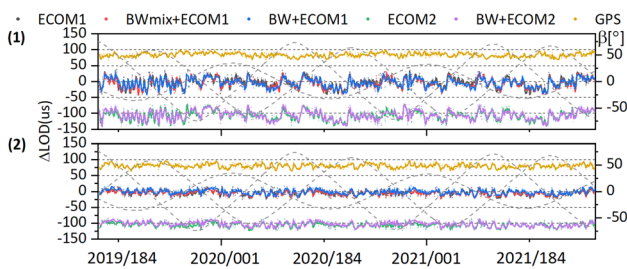

Fig. 9 Time series of Δ LOD differences with respect to IERS 14C04 product. (1) The 1 day arc solutions (2) The 3 day arc solutions. The ECOM2, BW+ECOM2, and GPS solutions are shifted by −100, −100 and 100 μs for a better display. Gray dashed lines denote the sun elevation angles above orbital planes

Table 9 Statistics of the Δ LOD differences with respect to IERS-C04-14

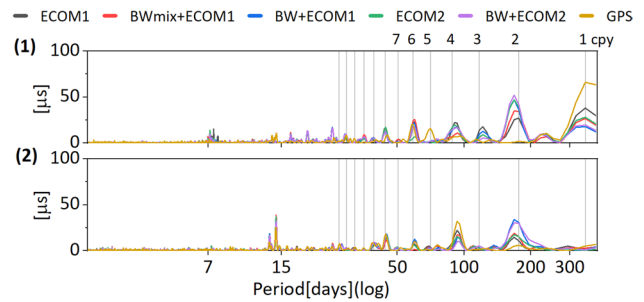|	1 day arc		3 day arc	
	Mean	STD	Mean	STD
Δ LOD (μs)				
ECOM1	−4	20	−5	9
ECOM2	−7	18	−5	9
BW+ECOM1	−5	18	−1	9
BW+ECOM2	−6	18	−3	10
BWmix+ECOM1	−6	18	−5	9
GPS	−16	8	−19	8

Fig. 10 Amplitude spectra of the differences of the estimated Δ LOD with respect to the IERS-C04-14 product. (1) The 1 day arc solutions (2) The 3 day arc solutions. The vertical gray lines represent the harmonics of a draconitic year

more significant than in pole coordinates and the amplitude exceeds 40 μas/day, especially when the related-ECOM1 is used. Interestingly, the spurious signals have almost completely vanished when turning to the 3 day arc. However, several signals in the high-frequency range (in particular over 3 days) are magnified.

In excess length of day processing, the UT1-UTC is tightly constrained to the IERS 14C04 values. Δ LOD can be estimated from GNSS. Figure 9 shows the time series of Δ LOD differences with respect to IERS 14C04 product and Table 9 also summarizes the mean offsets and STD values of the Δ LOD differences. An apparent degradation is identified at the *β* zero-crossing points for BDS 1 day solutions in Fig. 9. This dependency is eliminated when switching to the 3 day arc solutions. Significant offsets in the differences of GPS-based Δ LOD can be found for both

the 1 and 3 day solutions. The mean value of GPS-based Δ LOD is 3 times larger than BDS-based Δ LOD, which may relate to the strength of resonance between the earth's rotation and the orbital period (2:1 for GPS and 17:9 for BDS). Similar accuracy is obtained for the different SRP models for the BDS-based solutions. The STD of Δ LOD residuals from 3 day arc solutions is improved by approximately 50% than those derived from 1 day solutions, which is 9 μs and comparable with the results of GPS. Moreover, Fig. 10 shows the spectral analysis of the residuals between the estimated Δ LOD and the IERS 14C04 series. The Δ LOD residuals show particularly high amplitudes at the even harmonics of the draconitic year from 2nd to the 10th. In the case of 1 day arc solution, the signal at 2nd harmonics of draconitic year for BDS-derived Δ LOD estimates reaches about 40 μs, which is significantly larger than that for the GPS-derived. The 3 day arc is beneficial to the reduction of the most of the signals at harmonics of draconitic year for BDS. The signals at 1st harmonics of draconitic year have almost vanished in the 3 day arc solutions. The related period of about 14.2 and 14.8 days in all solutions may originate from the aliasing of the ocean constituents of O_1 and M_1 in the high-frequency pole model from IERS 2010, which is more visible in the 3 day arc

solutions and may be because of the error accumulation (Griffiths and Ray 2013).

Conclusion

ERPs are susceptible to absorbing the spurious effects from GNSS constellation characteristics and orbit modeling deficiencies, especially the deficiencies in the SRP models. The a priori box-wing model has been proved to reduce the spurious signals in Galileo-based ERP estimation. In this study, the properties of BDS satellite illuminated surfaces are firstly adjusted by the box-wing model and then jointly used with different empirical models in ERP estimation.

The estimated ERPs are compared to the reference values of the IERS 14C04 product. The mean offsets of BDS-derived ERPs using different SRP models are almost at the same level. However, the STD values are improved by approximately 20% for pole coordinates and their rates when the a priori box-wing model is applied for ECOM1. The improvement of the application of a priori box-wing model is slight for ECOM2. We identify the BW + ECOM1 ERP solution as the most reliable among all the other BDS solutions. In addition, the BDS-derived ERPs are affected by the system-specific spurious signals. The visible signals at the 3rd harmonics of the draconitic year in the pole coordinates may be related to the 3-plane constellations of BDS. The clear peaks at the 5th (about 70 days) and 7th (about 52 days) harmonics of the draconitic year can be identified as the repeating period of both β zero-crossing and equal β points for BDS. These signals are mitigated when the hybrid SRP modeling is applied. The orbit repeat period of BDS-3 MEO satellites leads to several pronounced peaks around 7 days in ERP estimation. The resonance between earth rotation and satellite revolution may introduce spurious signals with a period close to 7.4 days. The Δ LOD residuals show particularly high amplitudes at the even harmonics of the draconitic year from 2nd to the 10th. The signal at 2nd harmonics of draconitic year for BDS-derived Δ LOD estimates is significantly larger than that for the GPS-derived. Fortunately, the extension of the orbital arc in the BDS processing from 1 to 3 day is beneficial for ERP quality. Compared to 1 day arc solutions, when a 3 day arc is adopted, the improvement of the estimated quality is about 28, 15 and 50% for X-pole, Y-pole coordinates and Δ LOD, respectively. The STD is more than 3 times better than that of 1-day arc solutions for pole coordinate rates. Most of the system-specific spurious signals are mitigated when turning to the 3 day arc. Finally, the STD of the 3 day arc length BDS-derived ERPs with respect to the IERS 14C04 product reaches about 40 μas, 100 μas/day, 9 μs for pole coordinates, pole coordinate rates and Δ LOD, respectively.

References

Arnold D, Meindl M, Beutler G, Dach R, Schaer S, Lutz S, Prange L, Sośnica K, Mervart L, Jäggi A (2015) CODE's new solar radiation pressure model for GNSS orbit determination. J Geod 89(8):775–791. https://doi.org/10.1007/s00190-015-0814-4

Bizouard C, Lambert S, Gattano C, Becker O, Richard J (2019) The IERS EOP 14C04 solution for earth orientation parameters consistent with ITRF 2014. J Geod 93(5):621–633. https://doi.org/10.1007/s00190-018-1186-3

Boehm J, Niell A, Tregoning P, Schuh H (2006) Global mapping function (GMF): a new empirical mapping function based on numerical weather model data. Geophys Res Lett 33(7):L07304. https://doi.org/10.1029/2005GL02554

Boehm J, Heinkelmann R, Schuh H (2007) Short note: a global model of pressure and temperature for geodetic applications. J Geod 81(10):679–683. https://doi.org/10.1007/s00190-007-0135-3

Bury G, Zajdel R, Sośnica K (2019) Accounting for perturbing forces acting on Galileo using a box-wing model. GPS Solutions 23(3):74. https://doi.org/10.1007/s10291-019-0860-0

Bury G, Sośnica K, Zajdel R, Strugarek D (2020) Towards 1-cm galileo orbits-challenges in modeling of perturbing forces. J Geod 96(2):16. https://doi.org/10.1007/s00190-020-01342-2

Dilssner F, Springer T, Enderle W, 2011. GPS IIF yaw attitude control during eclipse season. In: AGU Fall Meeting, San Francisco. http://acc.igs.org/orbits/yaw-IIF_ESOC_agu11.pdf

Dilssner F, Laufer G, Springer T, Schönemann E, Enderle W, 2018. The BeiDou attitude model for continuous yawing MEO and IGSO spacecraft. In: EGU 2018, Vienna. http://navigation-office.esa.int/attachments_29393052_1_EGU2018_Dilssner_Final.pdf.

Duan B, Hugentobler U, Selmke I, Marz S, Killian M, Rott M (2022) BeiDou satellite radiation force models for precise orbit determination and geodetic applications. IEEE Trans Aerosp Electron Syst. https://doi.org/10.1109/TAES.2021.3140018

Griffiths J, Ray J (2013) Sub-daily alias and draconitic errors in the IGS orbits. GPS Solut 17(3):413–422. https://doi.org/10.1007/s10291-012-0289-1

Gross R, Fukumori I, Menementlis D (2003) Atmospheric and oceanic excitation of the earth's wobbles during 1980–2000. J Geophys Res Solid Earth 108(B8):2370. https://doi.org/10.1029/2002JB002143

Johnston G, Riddell A, Hausler G (2017) The international GNSS service. In: Teunissen PJG, Montenbruck O (eds) Springer handbook of global navigation satellite systems. Springer International Publishing, Berlin, pp 967–982. https://doi.org/10.1007/978-3-319-42928-1

Kouba J (2008) A simplified yaw-attitude model for eclipsing GPS satellites. GPS Solut 13(1):1–12. https://doi.org/10.1007/s10291-008-0092-1

Lutz S, Meindl M, Steigenberger P, Beutler G, Sośnica K, Schaer S, Dach R, Arnold D, Thaller D, Jaggi A (2016) Impact of the arc length on GNSS analysis results. J Geod 90(4):365–378. https://doi.org/10.1007/s00190-015-0878-1

Lyard F, Lefevre F, Letellier T, Francis O (2006) Modelling the global ocean tides: modern insights from FES2004. Ocean Dyn 56(5–6):394–415. https://doi.org/10.1007/s10236-006-0086-x

Montenbruck O et al (2017) The multi-GNSS experiment (MGEX) of the international GNSS service (IGS)–achievements, prospects and challenges. Adv Space Res 59(7):1671–1697. https://doi.org/10.1016/j.asr.2017.01.011

Petit G, Luzum B, 2010. IERS Conventions (2010). Frankfurt am Main: Verlag des Bundesamts für Kartographie und Geodäsie, 2010. 179 pp, ISBN 3–89888–989–6

Ray R, Steinberg D, Chao B, Cartwright D (1994) Diurnal and semidiurnal variations in the earth's rotation rate induced by ocean tides. Science 264:830–832. https://doi.org/10.1126/science.264.5160.830

Rebischung P, Schmid R, 2016. IGS14/igs14.atx: a new framework for the IGS Products. In: American geophysical union fall meeting 2016 San Francisco,USA. https://mediatum.ub.tum.de/doc/1341338/file.pdf

Rodriguez-Solano C, Hugentobler U, Steigenberger P (2012a) Adjustable box-wing model for solar radiation pressure impacting GPS satellites. Adv Space Res 49(7):1113–1128. https://doi.org/10.1016/j.asr.2012.01.016

Rodriguez-Solano C, Hugentobler U, Steigenberger P, Lutz S (2012b) Impact of Earth radiation pressure on GPS position estimates. J Geod 86(5):309–317. https://doi.org/10.1007/s00190-011-0517-4

Rodriguez-Solano C, Hugentobler U, Steigenberger P, Blossfeld M, Fritsche M (2014) Reducing the draconitic errors in GNSS geodetic products. J Geod 88(6):559–574. https://doi.org/10.1007/s00190-014-0704-1

Saastamoinen J (1972) Contribution to the theory of atmospheric refraction. B Geod 105(1):279–298. https://doi.org/10.1007/BF02521844

Scaramuzza S, Dach R, Beutler G, Arnold D, Sušnik A, Jäggi A (2018) Dependency of geodynamic parameters on the GNSS constellation. J Geod 92(1):93–104. https://doi.org/10.1007/s00190-017-1047-5

Springer T, Beutler G, Rothacher M (1999) Improving the orbit estimates of GPS satellites. J Geod 73(3):147–157. https://doi.org/10.1007/s001900050230

Steigenberger P, Thoelert S, Montenbruck O (2018) GNSS satellite transmit power and its impact on orbit determination. J Geod 92:609–624. https://doi.org/10.1007/s00190-017-1082-2

Steigenberger P, Thoelert S, 2020. Initial BDS-3 transmit power analysis (with BDS-2 gain pattern). https://files.igs.org/pub/station/general/igs_satellite_metadata.snx

Thaller D, Krügel M, Rothacher M, Tesmer V, Schmid R, Angermann D (2007) Combined Earth orientation parameters based on homogeneous and continuous VLBI and GPS data. J Geod 81(6–8):529–541. https://doi.org/10.1007/s00190-006-0115-z

Tianhe X, Sumei Y, Li J (2014) Earth rotation parameters determination using BDS and GPS data based on MGEX network. In: Sun J, Jiao W, Haitao W, Mingquan L (eds) China satellite navigation conference (CSNC) 2014 proceedings: volume III. Springer, Berlin, Heidelberg, pp 289–299. https://doi.org/10.1007/978-3-642-54740-9_26

Wang C, Guo J, Zhao Q, Ge M (2022) Improving the orbits of the BDS-2 IGSO and MEO satellites with compensating thermal radiation pressure parameters. Remote Sens 14(3):641. https://doi.org/10.3390/rs14030641

Wanninger L, Beer S (2015) BeiDou satellite-induced code pseudorange variations: diagnosis and therapy. GPS Solut 19(4):639–648. https://doi.org/10.1007/s10291-014-0423-3

Yang Y, Mao Y, Sun B, 2020. Basic performance and future developments of BeiDou global navigation satellite system. Satell Navig, 1,1 https://doi.org/10.1186/s43020-019-0006-0

Zajdel R, Sosnica K, Bury G, Dach R, Prange L, 2020. System-specific systematic errors in earth rotation parameters derived from GPS, GLONASS, and Galileo. GPS Solut, 24(3). https://doi.org/10.1007/s10291-020-00989-w

Zajdel R, Sosnica K, Bury G, 2021. Geocenter coordinates derived from multi-GNSS: a look into the role of solar radiation pressure modeling. GPS Solut, 25(1):1 https://doi.org/10.1007/s10291-020-01037-3

Zhao Q, Guo J, Wang C, Lv Y, Xu X, Yang C, Li J, 2022. Precise orbit determination for BDS satellites. Satell Navig, 3, 2 https://doi.org/10.1186/s43020-021-00062-y

Zou X, Li Z, Wang Y, Deng C, Li Y, Tang W, Ruinan F, Cui J, Liu J (2021) Multipath error fusion modeling methods for Multi-GNSS. Remote Sens 13(15):2925. https://doi.org/10.3390/rs13152925

Yaquan Peng is currently a PhD candidate at GNSS Research Center, Wuhan University. His current research mainly focuses on precise-orbit determination and its application for geosciences.
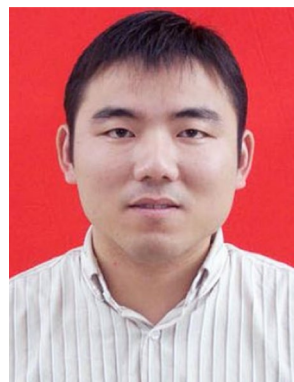
Yidong Lou received his PhD in Geodesy and Surveying Engineering from Wuhan University in 2008 and is a professor at GNSS Research Center, Wuhan University. His current research interest is in real-time precise GNSS orbit determination and real-time GNSS PPP.

Xiaolei Dai is currently an associate research fellow at Wuhan University. She received her PhD degree from Wuhan University in 2016. Her current research interests are real-time precise-orbit determination and clock estimation of GNSS, orbit attitude and force modeling for BDS and real-time data processing in the RTS system.

Chuang Shi is currently a professor at the research institute for frontier science, Beihang University. He graduated from the Wuhan Institute of Surveying and Mapping (current Wuhan University) and obtained his PhD in 1998. His research interests include network adjustment, precise orbit determination for GNSS satellites and LEOs, as well as real-time PPP.

Jing Guo is currently an associate professor at GNSS Research Center of Wuhan University. He received his bachelor, master and doctorate degrees at Wuhan University in 2009, 2011 and 2014, respectively. Currently, he works on GNSS data processing, particularly the precise orbit determination for multi-GNSS satellites, and is also responsible for the routine data processing of MGEX and iGMAS at Wuhan University.